Applied Surface Science 258 (2012) 9480–9483

Contents lists available at ScienceDirect

Applied Surface Science

journal homepage: www.elsevier.com/locate/apsusc

A wide-range model for simulation of pump-probe experiments with metals

Mikhail E. Povarnitsyn[a,*], Nikolay E. Andreev[a,b], Eugeny M. Apfelbaum[a], Tatiana E. Itina[a,c], Konstatntin V. Khishchenko[a,b], Oleg F. Kostenko[a], Pavel R. Levashov[a,b], Mikhail E. Veysman[a]

[a] Joint Institute for High Temperatures RAS, Izhorskaya 13 Bldg 2, Moscow, 125412, Russia
[b] Moscow Institute of Physics and Technology (State University), Institutsky lane 9, Dolgoprudny, Moscow region, 141700, Russia
[c] Laboratoire Hubert Curien, UMR CNRS 5516, 18 rue Benoît Lauras, Bât. F, 42000, St-Etienne, France

ARTICLE INFO

Article history:
Available online 8 July 2011

Keywords:
Laser-metal interaction
Pump-probe experiment
Phase shift
Transport properties

ABSTRACT

High precision pump-probe experiments can provide a valuable information about material states out of equilibrium. A wide-range numerical model is used for the description of material response on ultra-short laser action. The model is developed on the basis of two-temperature hydrodynamics with heat transport, ionization, plasma expansion, electron-ion collisions and two-temperature equation of state for an irradiated substance. Comparison of experimental findings with the results of simulation is used both for the numerical model verification and for calculation of plasma thermodynamic parameters that cannot be measured directly in experiment. An aluminum target is heated by an intense 400 nm (2ω) pump laser pulse that is incident normal to the planar target. Weak *S*- and *P*-polarized probe pulses with wavelength 800 nm (1ω) are used for diagnostics of the plasma. Both probe pulses illuminate the target at a 45° angle. Calculation of the reflectivity and phase shift of probe pulses with both polarizations are in good agreement with experiment.

1. Introduction

Intense subpicosecond laser heating of solid metal targets produces states with high temperatures (tens of eV) and near-normal densities. Such plasma conditions were studied experimentally with a femtosecond optical probe technique [1,2]. The time evolution of reflectivity showed the material response on laser action and fast changes of optical properties. The phase shift measurements can also be useful for the determination of optical properties at short delays after the material heating and plasma motion for long enough delays. In general, for adequate description of laser-irradiated target and the temporal evolution of its characteristic features, wide-range models of optical, transport and thermodynamic properties of matter are necessary. The role of modeling in this case is particularly important, since the strong inhomogeneity of the produced plasma and its fast evolution do not permit direct measurements of plasma properties.

2. Governing equations

Equations for conservation of mass, momentum and energy for electron and ion subsystems can be written in one-velocity two-temperature 1D Lagrangian form as follows

$$\frac{\partial V}{\partial t} - \frac{\partial u}{\partial m} = 0, \tag{1}$$

$$\frac{\partial u}{\partial t} + \frac{\partial (P_\mathrm{i} + P_\mathrm{e})}{\partial m} = 0, \tag{2}$$

$$\frac{\partial e_\mathrm{e}}{\partial t} + P_\mathrm{e}\frac{\partial u}{\partial m} = -\gamma_\mathrm{ei}(T_\mathrm{e} - T_\mathrm{i})V + Q_\mathrm{L}V + \frac{\partial}{\partial m}\left(\kappa\frac{\partial T_\mathrm{e}}{\partial z}\right), \tag{3}$$

$$\frac{\partial e_\mathrm{i}}{\partial t} + P_\mathrm{i}\frac{\partial u}{\partial m} = \gamma_\mathrm{ei}(T_\mathrm{e} - T_\mathrm{i})V. \tag{4}$$

Here V is the material specific volume; m is the mass coordinate; t is the time; z is the space coordinate; u is the velocity; P_e and P_i are the pressures of electrons and ions, respectively; e_e and e_i are the specific energies of electrons and ions, respectively. The electron–phonon/ion energy coupling is described by the coefficient γ_ei. The laser energy absorption by the conduction band electrons is taken into account by the term Q_L. Electron thermal conductivity coefficient κ is used for the description of heat transport in Fourier form. The temperatures of electrons and ions are T_e and T_i, respectively. Similar model in Eulerian form is discussed in detail in our previous paper [3]. Below we show that one-velocity two-temperature hydrodynamic approach, although approximate, gives reasonable agreement with experimental data.

* Corresponding author.
E-mail address: povar@ihed.ras.ru (M.E. Povarnitsyn).

0169-4332/$ – see front matter © 2011 Elsevier B.V. All rights reserved.
doi:10.1016/j.apsusc.2011.07.017

3. Equation of state

We use the two-temperature multi-phase equation of state (EOS) for Al with special treatment of metastable states [4,5]. The peculiarity of this work is in the Thomas–Fermi expression for the thermal contribution of electrons [6] instead of the ideal Fermi-gas one. This is essential for the correct description of laser energy absorption.

4. Transport properties

The material response to the laser action is based on the oscillation of electrons in the laser field. In metals, the conduction band electrons are considered as fluid. The properties of matter in this case may be described by the Drude model for temperatures below the Fermi one T_F. In some metals band-to-band contribution ε_{bb} to permittivity may be dominant [7]. In the present model the metallic part ε_{met} is the sum of the band-to-band contribution and the intraband Drude-like term,

$$\varepsilon_{met}(\omega_L, \rho, T_i, T_e) = \varepsilon_{bb} + 1 - \frac{n_e}{n_{cr}(1 + i\nu_{eff,p}/\omega_L)}, \quad (5)$$

where n_e and n_{cr} are the electron concentration and the critical one, respectively, and ω_L is the laser frequency. The effective frequency of collisions is $\nu_{eff,p} = \min(\nu_{met,p}, \nu_{max,p})$.

The frequency of collisions in metal state is a sum of electron–phonon and electron–electron collisions

$$\nu_{met,p} = \frac{A_1^p k_B T_i}{\hbar} + \frac{A_2^p k_B T_e^2}{(T_F \hbar)}. \quad (6)$$

The maximal frequency of collisions corresponds to electron free-path between ions (interatomic distance r_0) so that

$$\nu_{max,p} = \frac{A_3^p}{r_0}\sqrt{\frac{v_F^2 + k_B T_e}{m_e}}, \quad (7)$$

where v_F is the Fermi speed of electrons.

For hot states $T_e >> T_F$ the plasma model is relevant as follows

$$\varepsilon_{pl}(\omega_L, \rho, T_e) = 1 - \frac{n_e}{n_{cr}}\left[K_1(\xi) - i\left(\frac{\nu_{pl}}{\omega_L}\right)K_2(\xi)\right]. \quad (8)$$

Here functions $K_1(\xi), K_2(\xi)$ with $\xi = 3\sqrt{\pi}\nu_{pl}/(4\omega_L)$ are described in Ref. [8]. Expression for plasma frequency has a form

$$\nu_{pl} = \frac{4}{3}\sqrt{2\pi}\frac{Z n_e e^4 \Lambda}{\sqrt{m_e}(k_B T_e)^{3/2}} \quad (9)$$

with mean charge of ions Z and Coulomb logarithm Λ.

We suppose that the metal–plasma transition occurs in the vicinity of the Fermi temperature and thus we can interpolate between these two states to obtain the wide-range model of permittivity $\varepsilon(\omega_L, \rho, T_i, T_e)$ which can be written as

$$\varepsilon = \varepsilon_{pl} + (\varepsilon_{met} - \varepsilon_{pl})e^{-A_4^p T_e/T_F}. \quad (10)$$

In Fig. 1 the permittivity (10) is presented for two laser wavelengths, 0.8 and 0.4 μm. The coefficients used in the permittivity model are adjusted to meet the room temperature conditions for aluminum [13] ($A_1^p = 4.41$) and describe experiments on self-reflectivity [14] ($A_2^p = 0.8$ and $A_3^p = 0.7$, $A_4^p = 0.2$).

The electron thermal conductivity in metal is calculated according to the Drude formalism as follows

$$\kappa_{met} = \frac{\pi^2 k_B^2 n_e}{3 m_e \nu_{eff,t}} T_e, \quad (11)$$

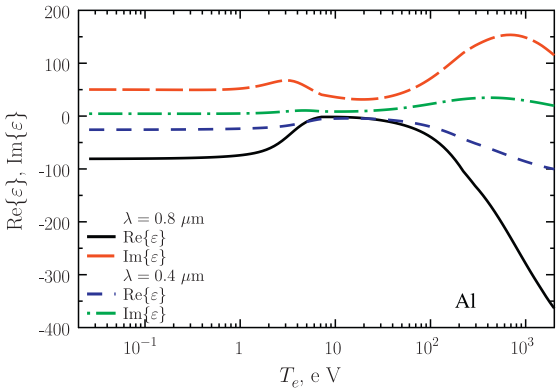

Fig. 1. Interpolation formula (10) for real and imaginary parts of permittivity for normal density of aluminum and two wavelengths 0.8 and 0.4 μm, $T_i = 293$ K.

and the hot plasma limit is

$$\kappa_{pl} = \frac{16\sqrt{2}k_B(k_B T_e)^{5/2}}{\pi^{3/2} Z e^4 \sqrt{m_e}\Lambda}. \quad (12)$$

An interpolation between (11) and (12) gives us a wide-range expression for thermal conductivity,

$$\kappa = \kappa_{pl} + (\kappa_{met} - \kappa_{pl})e^{-A_4^t T_e/T_F}, \quad (13)$$

where $A_4^t = 1.2$. The corresponding effective frequency has a form $\nu_{eff,t} = \min(\nu_{met,t}, \nu_{max,t})$. The expressions for $\nu_{met,t}$ and $\nu_{max,t}$ are similar to (6) and (7), respectively, with corresponding coefficients $A_1^t = 2.95$, $A_2^t = 0.5$ and $A_3^t = 0.16$. In Fig. 2, we compare the results of the interpolation (13) with the theoretical data [9–11] for normal and 0.1 of normal density.

Finally, for the coupling parameter we use the following equation

$$\gamma_{ei} = \frac{3k_B m_e}{m_i} n_e \nu_{eff,g}, \quad (14)$$

where $\nu_{eff,g} = \min(\nu_{met,g}, \nu_{max,g}, \nu_{pl})$ is given by expressions (6), (7) and (9) with material coefficients $A_1^g = 50.0$, $A_2^g = 20.0$, $A_3^g = 0.25$. The coupling factor (14) and results of first-principle calculations [12] are presented in Fig. 3.

5. Laser energy absorption and reflection

In general, laser light absorption and reflection can be calculated for an arbitrary profile of high-frequency permittivity. As was

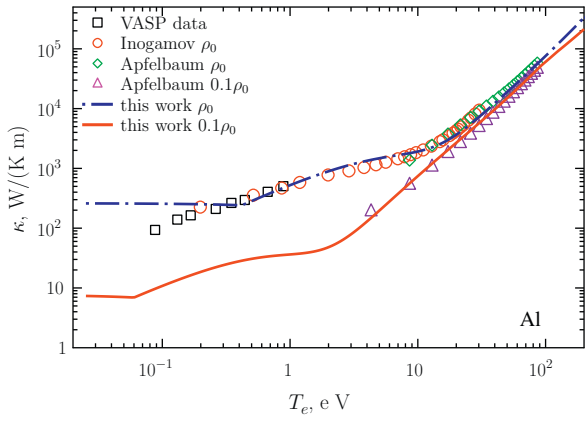

Fig. 2. Comparison of interpolation formula (13) with available theoretical data of VASP [9], Inogamov et al. [10], Apfelbaum [11] for thermal conductivity in cases of normal and 0.1 of normal densities of aluminum, $T_i = T_e$.

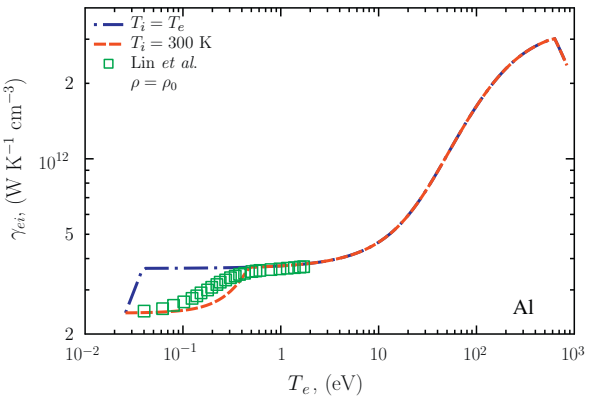

Fig. 3. Wide-range model for energy exchange coefficient according to formula (14) and theoretical results of Lin et al. [12] for normal density of aluminum.

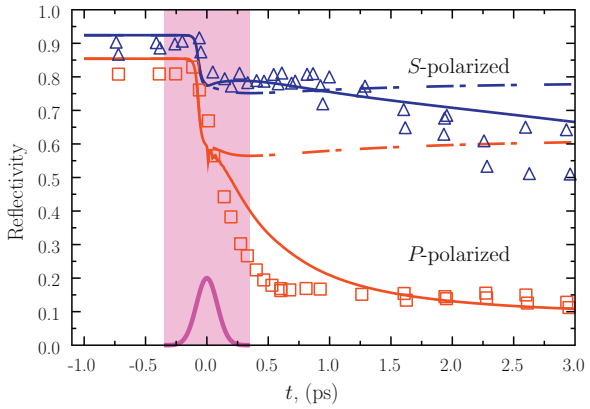

Fig. 4. Experimental reflectivity dynamics for the *S*- (blue triangles) and the *P*-polarized (red squares) probe pulses. Corresponding simulation results are presented by the blue and red solid lines, respectively. Dash-and-dot lines show the reflectivity changes for "frozen motion" regime. The pump pulse profile is also presented. (For interpretation of the references to color in this figure legend, the reader is referred to the web version of the article.)

shown in the previous section, the permittivity is a function of thermodynamic parameters, which in turn can be calculated with the space resolution used in the hydrodynamic part of the model. Then, the laser interaction is governed by several characteristic scales such as wavelength, skin layer, and also resonance absorption layer for *P*-polarized beam.

Let us suppose that permittivity depends on z coordinate only $\varepsilon = \varepsilon(z)$ and $\varepsilon(z \to -\infty) = 1$. Then, for *S*-polarization, we can write $\tilde{\mathbf{E}} = \mathrm{Re}\{\mathbf{E}\exp(-i\omega_L t + ik_0 x \sin\theta)\}$, $\mathbf{E} = \{0, E_y, 0\}$, $\mathbf{k_0} = (\omega_L/c)\{\sin\theta, 0, \cos\theta\}$. For the single component of electric laser field envelope $E(z, t) \equiv E_y(z, t)$ slowly changing in time one can write

$$\frac{\partial^2 E}{\partial z^2} + k_0^2[\varepsilon(z) - \sin^2\theta]E = 0. \tag{15}$$

In the case of *P*-polarization the single component of magnetic field envelope $B(z, t) \equiv B_y(z, t)$, $\mathbf{B} = \{0, B_y, 0\}$, obeys the following equation,

$$\frac{\partial^2 B}{\partial z^2} + k_0^2[\varepsilon(z) - \sin^2\theta]B - \frac{\ln\varepsilon(z)}{\partial z}\frac{\partial B}{\partial z} = 0. \tag{16}$$

By using the transfer-matrix method [15] one can find the space distribution of electromagnetic field. This distribution determines the laser energy deposition Q_L into the target in electron energy Eq. (3):

$$Q_L(z) = \frac{\omega_L}{8\pi}\mathrm{Im}\{\varepsilon(z)\}|\mathbf{E}(z)|^2, \tag{17}$$

where

$$|\mathbf{E}|^2 = \begin{cases} |E_y|^2, & \text{if } S\text{-polarized}, \\ |E_x|^2 + |E_z|^2, & \text{if } P\text{-polarized}. \end{cases} \tag{18}$$

The components of the electric field for *P*-polarization case can be calculated from the equations $E_z = -B_y \sin\theta/\varepsilon$, $E_x = -i/(\varepsilon k_0)(\partial B_y/\partial z)$.

6. Results and discussion

Series of simulations are performed for the experiment of Ref. [1] by using the model described above. In the experiment the bulk aluminum target was heated by normal incident laser pulse with intensity 10^{14} W/cm^2, laser wavelength 400 nm and full width at half maximum (FWHM) 120 fs. Two probe pulses with FWHM 110 fs, 800 nm wavelength and angle of incidence 45° were used for aluminum plasma diagnostics. The intensity of probe pulses did not disturb the target parameters. For the pump pulse as well as for the probe ones we solve the equations of electromagnetic field (15) and (16) with the permittivity profile that is a function of time and space dependent thermodynamic parameters determined by equations (1)–(4). The results of the solution to Eqs. (15) and (16) are the electromagnetic field distribution as well as the reflectivity and phase shift evolution for *S*- and *P*-polarized probe pulses.

A comparison of the simulation results with the experimentally measured reflectivity is presented in Fig. 4. One can see in the Figure that the reflectivity drops during the pump pulse action. After that, the rarefaction of near-surface material layers starts leading to a subsequent decay in reflectivity both for *S*- and *P*-polarized probe pulse. The role of the target material motion is illustrated by comparison of the solid curves with the dash-and-dot ones that are obtained in the regime of "frozen motion" ($u \equiv 0$).

The phase shift is presented in Fig. 5. During the pump pulse, the phase shift takes place due to the transport property changes in the bulk of the target. Then, the phase changes occur mainly because of the material motion. Under discussed conditions the absorption of the *P*-polarized probe takes place in the vicinity of the critical concentration n_{cr} (resonance absorption), whereas the *S*-polarized pulse is absorbed mainly at the position corresponding to the electron concentration of $n_{cr}\cos^2\theta$. The difference in these S and P-polarized phase shifts can be explained by the growing distance between the locations of these two concentrations and by the decay in the electron concentration gradient.

An increase of the laser absorption (the drop of reflectivity) in the real case of the material motion is caused mainly by the rarefaction and increasing of the characteristic density scale length

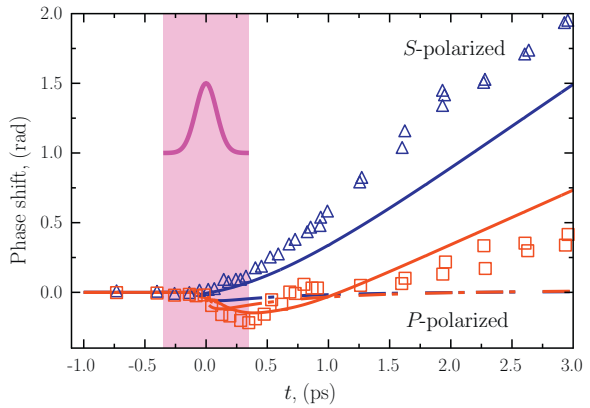

Fig. 5. Experimental phase-shift dynamics, denotations as in Fig. 4.

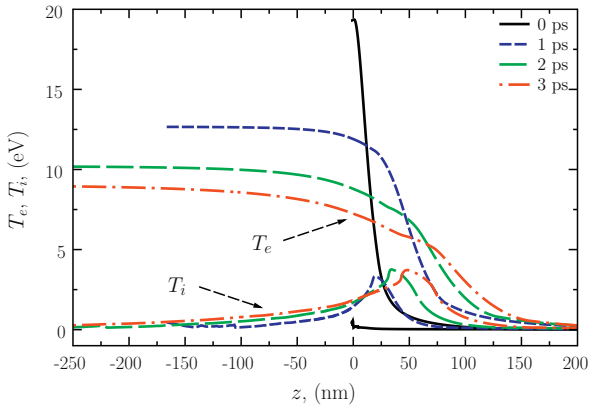

Fig. 6. Temperature of electrons and ions for different moments, 0 ps corresponds to the peak intensity of the pump pulse. Pulses travel from the left, initial target surface position at $z = 0$.

at the critical electron plasma density. For *S*-polarized probe pulse the increase in absorption is a consequence of the growth of the absorption region, and so is more pronounced at the longer time delay. For the *P*-polarized probe, the appearance of the finite density gradient leads to switching on the resonant absorption, and so to earlier and stronger drop in the reflection.

The temperature of electrons and ions for different time moments is shown in Fig. 6 demonstrating strong inhomogeneity of parameters in the target. One can clearly see that the transport properties are governed mainly by electron excitation at 0 ps (maximum of the pump pulse). At that time, electron temperature reaches 20 eV, while the temperature of ions is still small. After that, the temperature of ions increases due to the electron-ion coupling effect and the ion temperature maximum moves into the bulk passing from $z = 25$ nm position at 1 ps moment to $z = 50$ nm for 3 ps delay. We note here that the discrepancy in the phase shift can be attributed to the target surface untidiness (oxide films etc.) and uncertainty in the measurement of laser pulse intensity in experiment. Both these facts may result in phase shift changes. Additional investigations and comparison with similar experimental data can give a valid answer to this question.

7. Conclusions

In summary, we have developed a wide-range model for realistic simulations of pump-probe experiments with metals. The model is capable to predict both reflectivity and the phase shift measured in typical experiments. The calculation results show the importance of the material motion in the model. In fact, it is crucial to account for the target material motion both during and after the pump pulse. In particular, the difference in phase shift obtained for *S*- and *P*-polarized probes can be used for the estimation of the electron concentration and its time-evolution.

8. Acknowledgments

This work is supported by the Presidium of the Russian Academy of Sciences (programs of basic researches), the Centre National de la Recherche Scientifique and the Russian Academy of Sciences (collaboration project No. 21276), the Russian Foundation for Basic Research (grants No. 09-08-01129, 11-02-91058-CNRS, 11-02-01457), the Council of the President of the Russian Federation for Support of Young Russian Scientists and Leading Scientific Schools (project No. NSh-65792.2010.2) and the Ministry of Education and Science of the Russian Federation (the Federal targeted program "Scientific and scientific-pedagogical personnel of the innovative Russia" 2009–2013).

References

[1] K. Widmann, et al., Phys. Plasmas 8 (2001) 3869–3872.
[2] M.B. Agranat, et al., J. Exp. Theor. Phys. Lett. 85 (2007) 271–276.
[3] M.E. Povarnitsyn, T.E. Itina, P.R. Levashov, K.V. Khishchenko, Appl. Surf. Sci. 253 (2007) 6343–6346.
[4] M.E. Povarnitsyn, T.E. Itina, M. Sentis, P.R. Levashov, K.V. Khishchenko, Phys. Rev. B 75 (2007) 235414.
[5] M.E. Povarnitsyn, K.V. Khishchenko, P.R. Levashov, Appl. Surf. Sci. 255 (2009) 5120–5124.
[6] O.P. Shemyakin, P.R. Levashov, L.R. Obruchkova, K.V. Khishchenko, J. Phys. A: Math. Theor. 43 (2010) 335003.
[7] B. Hüttner, J. Phys.: Cond. Matter 8 (1996) 11041.
[8] M. Veysman, B. Cros, N. Andreev, G. Maynard, Phys. Plasma 13 (2006) 053114.
[9] V. Recoules, J.-P. Crocombette, Phys. Rev. B 72 (2005) 104202.
[10] N. Inogamov, Y. Petrov, J. Exp. Theor. Phys. 110 (2010) 446–468.
[11] E.M. Apfelbaum, High Temp.: High Press. 37 (2008) 253–260.
[12] Z. Lin, L.V. Zhigilei, V. Celli, Phys. Rev. B 77 (2008) 075133.
[13] E.D. Palik, Handbook of Optical Constants of Solids I , Academic Press, 1985.
[14] D.F. Price, et al., Phys. Rev. Lett. 75 (1995) 252–255.
[15] M. Born, E. Wolf, Principles of optics , 7th edition, Cambridge University Press, 1999.